Microchimica Acta (2024) 191:263
https://doi.org/10.1007/s00604-024-06348-7

ORIGINAL PAPER

A metal–organic framework and quantum dot-based ratiometric fluorescent probe for the detection of formaldehyde in food

Chen Chen[1] · Zhigang Liang[1] · Xinyang Li[1] · Feifei Xu[1] · Guanhong Xu[1,2] · Fangdi Wei[1,2] · Jing Yang[1,2] · Qin Hu[1,2] · Yao Cen[1,2,3]

Received: 27 February 2024 / Accepted: 4 April 2024 / Published online: 15 April 2024

Abstract

A green and sensitive ratio fluorescence strategy was proposed for the detection of formaldehyde (FA) in food based on a kind of metal–organic frameworks (MOFs), MIL-53(Fe)-NO_2, and nitrogen-doped Ti_3C_2 MXene quantum dots (N-Ti_3C_2 MQDs) with a blue fluorescence at 450 nm. As a type of MOFs with oxidase-like activity, MIL-53(Fe)-NO_2 can catalyze *o*-phenylenediamine (OPD) into yellow fluorescent product 2,3-diaminophenazine (DAP) with a fluorescent emission at 560 nm. DAP has the ability to suppress the blue light of N-Ti_3C_2 MQDs due to inner filter effect (IFE). Nevertheless, Schiff base reaction can occur between FA and OPD, inhibiting DAP production. This results in a weakening of the IFE which reverses the original fluorescence color and intensity of DAP and N-Ti_3C_2 MQDs. So, the ratio of fluorescence intensity detected at respective 450 nm and 560 nm was designed as the readout signal to detect FA in food. The linear range of FA detection was 1–200 μM, with a limit of detection of 0.49 μM. The method developed was successfully used to detect FA in food with satisfactory results. It indicates that MIL-53(Fe)-NO_2, OPD, and N-Ti_3C_2 MQDs (MON) system constructed by integrating the mimics enzyme, enzyme substrate, and fluorescent quantum dots has potential application for FA detection in practical samples.

Keywords Metal–organic frameworks · Oxidase-mimicking activity · Inner filter effect · Schiff base reaction

Introduction

Formaldehyde (FA) in the environment is a harmful gas, and its liquid state is called formalin [1]. As one of the most feared carcinogenic and mutagenic pollutants, FA has a great killing power [2]. Unfortunately, FA is often illegally added in food for preservative, fresh-keeping, bleaching, and other functions [3, 4]. Excessive intake of FA can cause vomiting, abdominal pain, fainting, and death in severe cases, and is included in the list of a class of carcinogens by the World Health Organization [5]. Therefore, it is very important to monitor FA in food.

Typical FA detection strategies rely on liquid chromatography [6] and spectrophotometry [7]. Liquid chromatography has the characteristics of high selectivity and high sensitivity, but costs much, and wastes time, especially needs professional operator. Spectrophotometry has the advantages of easy operating, economic, and wide linear range, but its selectivity and sensitivity are poor. In recent years, colorimetry [8], surface-enhanced Raman spectroscopy [9], electrochemical [10], and fluorescent [11] methods have gradually emerged. Among them, fluorescence technology is favored because of its preponderances like uncomplicated operation, high sensitivity, and short time [12]. Various fluorescent probes have been explored for the sensing of FA, such as quantum dots (QDs) [13], organic small molecules [14], metal nanoparticles [15], and metal–organic frameworks (MOFs) [16].

✉ Qin Hu
huqin@njmu.edu.cn

✉ Yao Cen
yaocen@njmu.edu.cn

1 School of Pharmacy, Nanjing Medical University, Nanjing, Jiangsu 211166, People's Republic of China

2 Key Laboratory of Cardiovascular & Cerebrovascular Medicine, School of Pharmacy, Nanjing Medical University, Nanjing, Jiangsu 211166, People's Republic of China

3 Shandong Key Laboratory of Biochemical Analysis, College of Chemistry and Molecular Engineering, Qingdao University of Science and Technology, Qingdao, Shandong 266042, People's Republic of China

Nevertheless, most studies have focused on direct luminescence sensing of FA in the gas phase, and these probes are usually complicated and ungreen. Moreover, the reported analytical methods could only detect FA at high concentration in samples. It is important to note that most fluorometric methods focus on single signal detection, which is susceptible to interference by equipment, operation, and environment. Ratio fluorescent sensors can calibrate these issues effectively [17]. Therefore, we attempted to construct a simple and green ratio fluorescence probe to detect FA in solution sensitively.

The rapid development of nanomaterials provides broad ways for the synthesis of simple and environmentally friendly detection probes [18]. As an important branch of nanomaterials, nanozymes were widely used in sensing, treatment, food safety, and environmental treatment due to their simple preparation, good stability, and diversity of properties [19, 20]. MOFs are ordered network structures formed by the self-assembly of organic ligands and metal ions [21]. Based on the MIL-53(Fe), the researchers found that MOFs with electron-absorbing substituents have strong enzyme-like activity especially MIL-53(Fe)-NO_2 [22]. To the best of our knowledge, there is no work utilizing MIL-53(Fe)-NO_2 to develop detection probes. In order to construct an ideal ratio fluorescence probe, we set our sights on QDs. Two-dimensional nanosheets are often an important source of new QDs, of which MXenes showed wonderful potential in the area of catalysis, adsorption, hydrogen storage, and sensing [23] due to their typical planar morphology, good surface properties, and excellent electrical conductivity [24]. QDs prepared with MXenes are often referred to as the MXene QDs (MQDs). MQDs not only inherit the inherent advantages of MXenes but also exhibit extraordinary photoelectric performance. In particular, the use of heteroatom-doped MQDs further improves the surface properties of MQDs [25]. Therefore, the exploration of heteroatomic-doped MQDs for fluorescence sensing of FA is very promising.

Herein, we pioneered MIL-53(Fe)-NO_2, *o*-phenylenediamine (OPD), and N-doped Ti_3C_2 MQDs (N-Ti_3C_2 MQDs) (MON) system to detect FA. To the best of our knowledge, there are no ratiometric fluorescent probes based on MOFs and QDs for FA detection. In the MON system, the substrate OPD was catalyzed by MIL-53(Fe)-NO_2 to produce the yellow fluorescent product 2,3-diaminophenazine (DAP). DAP can quench the blue fluorescence of N-Ti_3C_2 MQDs due to the internal filtering effect (IFE). In the presence of FA, the amount of OPD in the system was changed and the original fluorescence color and intensity were reversed based on the specific Schiff base reaction. In light of the aforementioned description, a ratio fluorescence probe was created. The analytical method for FA detection in food samples was also validated.

Experimental section

Materials

2-nitro-1,4-benzenedicarboxylic acid (NO_2-BDC, 98%), ethylenediaminetetraacetic acid (EDTA), zinc acetate ($Zn(AcO)_2{\cdot}2H_2O$, 99%), iron (III) chloride hexahydrate ($FeCl_3{\cdot}6H_2O$, 99%), *o*-phenylenediamine (OPD, 99%), histidine (His, 99%), 2,4-dinitrophenylhydrazine (DNPH, 98%), formaldehyde standard solution (100 $mg{\cdot}L^{-1}$), and potassium ferrocyanide trihydrate ($K_4Fe(CN)_6{\cdot}3H_2O$, 99%) were purchased from Aladdin Industrial Corporation (Shanghai, China). Ti_3C_2 MXene was purchased from XFNANO Materials Tech Co. (Nanjing, China). Diethylenetriamine (DETA), isopropanol (IPA), N, N-dimethylformamide (DMF), sodium acetate (NaAc), and formaldehyde (FA, 37%) were purchased from Sinopharm Chemical Reagent Co., Ltd. (Shanghai, China). p-Benzoquinone (BQ, 99%) was purchased from Shanghai Titan Technology Co., Ltd. (Shanghai, China). All other chemicals used in this work were of analytical grade and used without further purification. Ultrapure water was obtained using a Milli-Q system (Millipore, USA).

Synthesis of MIL-53(Fe)-NO_2 and N-Ti_3C_2 MQDs

MIL-53(Fe)-NO_2 was synthesized with reference to previous work [22]. N-Ti_3C_2 MQDs was synthesized by slightly modifying existing work [26]. The specific synthesis steps of these materials were described in detail in the Supplementary Material.

Evaluation of the oxidase-mimicking activity of MIL-53(Fe)-NO_2

Briefly, 40 µL of 100 $\mu g{\cdot}mL^{-1}$ MIL-53(Fe)-NO_2, 20 µL of 500 mM NaAc buffer (pH = 4.5), 10 µL of 0.4 mM OPD, and 30 µL deionized water were mixed. The UV–vis absorption spectrum at 350–550 nm was recorded after a 40-min reaction at 37 °C.

Oxidase-mimicking catalytic mechanism of MIL-53(Fe)-NO_2

To verify whether O_2 participated in the catalytic reaction, N_2 was blown into the mixture of OPD and MIL-53(Fe)-NO_2 for 10 min to remove O_2 dissolved in the solution, and then the UV–vis absorption spectra was measured.

Dissolved oxygen plays a crucial role in the reactions catalyzed by oxidases. We explored the reactive oxygen species that might be present throughout the system. In the

mixture of 40 μL of 100 μg·mL^{-1} MIL-53(Fe)-NO_2, 10 μL of 0.4 mM OPD, 20 μL 500 mM NaAc buffer (pH = 4.5), and 20 μL deionized water, 10 μL of IPA, His, BQ, and EDTA with different concentrations were added and reacted for 2 h. The UV–vis absorption spectra of 350–550 nm were obtained.

Determination of FA

In short, 10 μL of 0.4 mM OPD and 10 μL of FA solution were added, and the combination was then incubated for 30 min at 37 °C. The system was then given 20 μL of 500 mM NaAc buffer (pH = 4.5), 40 μL of 100 μg·mL^{-1} MIL-53(Fe)-NO_2, 5 μL of N-Ti_3C_2 MQDs, and 15 μL of ultrapure water. Following a thorough mixing of the solution and a 40-min incubation period at 37 °C, the fluorescence was measured.

Real food sample analysis

All food samples were bought from the Suguo supermarket in Nanjing, China. The beer was allowed to set for 2 h to eliminate air bubbles and then directly tested for FA using the same procedure as in the "Determination of FA" section.

Food samples such as cabbage, mushroom, and frozen shrimp needed further processing. Two grams of each sample was chopped and soaked in 8 mL deionized water. To eliminate proteins, 1 mL of $K_4Fe(CN)_6{\cdot}3H_2O$ (100 mM) and 1 mL of $Zn(AcO)_2{\cdot}2H_2O$ (100 mM) were added. After 20 min of ultrasonic treatment, the mixture was centrifuged at 0 °C. The food extraction liquid was obtained by centrifugation and filtration. FA concentration was measured using the method described above.

High performance liquid chromatography (HPLC) experiments

The national standard for food safety stipulates that spectrophotometry and liquid chromatography are the gold standards for the detection of FA in food. Here we chose HPLC as the standard method for comparison. Detailed HPLC conditions were provided in the Supplementary Material. FA concentrations in blank and sample solutions were obtained by HPLC standard curve method.

Results and discussion

Characterization of MIL-53(Fe)-NO_2

Transmission electron microscopy (TEM) and scanning electron microscopy (SEM) were used to describe the morphology of MIL-53(Fe)-NO_2. As depicted in Fig. 1A and B, MIL-53(Fe)-NO_2 had an octahedral crystal structure, which was consistent with literature reports [22]. Fourier transform infrared spectroscopy (FT-IR) was used to pinpoint the distinctive functional groups of MIL-53(Fe)-NO_2 (Fig. S1A). In addition, X-ray photoelectron spectroscopy (XPS) was used to confirm that MIL-53(Fe)-NO_2 was composed the components of Fe, O, N, and C (Fig. S1B). The characterization data mentioned above indicated that MIL-53(Fe)-NO_2 was successfully synthesized [27–29].

We selected OPD to assess the oxidase simulation activity of MIL-53(Fe)-NO_2. When both OPD and MIL-53(Fe)-NO_2 were present in the system, significant absorption occurred in the range of 350–550 nm, indicating that OPD was oxidized to DAP (Fig. 1C). This demonstrated that MIL-53(Fe)-NO_2 could successfully catalyze OPD oxidation without supplementary oxidant. At the same time, we explored the optimal pH for MIL-53(Fe)-NO_2 activity. Figure S2A showed that in the range of pH 3.0–5.5, the fluorescence intensity first increases and then decreases, reaching a peak value at pH 4.5. In addition, MIL-53(Fe)-NO_2 still had a considerable ability to catalyze the oxidation of OPD to DAP when stored at room temperature for 10 days (Fig. S2B).

It is known that in catalytic oxidation reaction systems, oxidases generate reactive oxygen species through dissolved oxygen to further oxidize substrates. To shed light on MIL-53(Fe)-NO_2's function in OPD oxidation, we conducted comparative experiments under nitrogen atmosphere. As shown in Fig. S3, with the introduction of N_2 into the solution, the reactive oxygen species produced decreased, resulting in a significant decrease in the absorbance of DAP, which demonstrated that the catalytic oxidation of OPD involved dissolved oxygen. To further explore the catalytic mechanism of OPD oxidation mediated, we selected different free radical scavengers. Generally, we used IPA, His, BQ, and EDTA as scavengers of hydroxyl radical (·OH), singlet oxygen ($^1O_2$), superoxide anion radical ($O_2^{\cdot-}$), and oxygen vacancy, respectively. As shown in Fig. 1D, in the presence of BQ and EDTA, the activity of the oxidase-mimicking enzyme MIL-53(Fe)-NO_2 significantly decreased, indicating that both superoxide anion radicals and oxygen vacancies participated in the catalytic reaction. Furthermore, $O_2^{\cdot-}$ was identified by electron paramagnetic resonance with 5,5-dimethyl-1-pyrroline N-oxide as the spin probe which further corroborated the results we obtained [30].

Characterization of N-Ti_3C_2 MQDs

TEM featured the morphology of N-Ti_3C_2 MQDs. Figure 2A indicated that N-Ti_3C_2 MQDs were spherical and uniformly dispersed in water medium. HRTEM diagram exposed the crystal characteristics of N-Ti_3C_2 MQDs. We can observe that the adjacent lattice fringes were 0.21 nm, in accord with the (0110) faces of the MXene [31]. To characterize

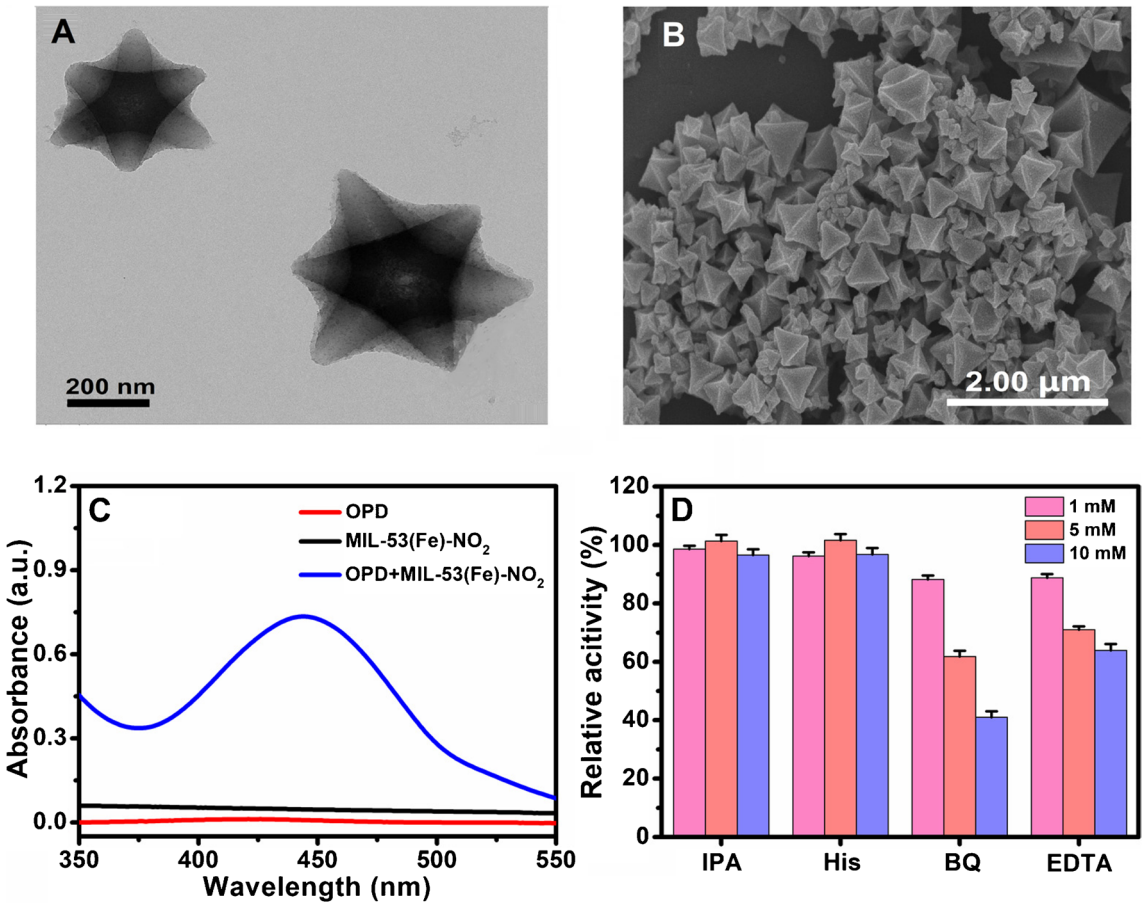

Fig. 1 **A** TEM image and **B** SEM image spectrum of MIL-53(Fe)-NO_2. **C** The UV–vis spectra of MIL-53(Fe)-NO_2-induced OPD oxidation. **D** Free radical capture test of MIL-53(Fe)-NO_2 ($n = 3$)

the size of N-Ti_3C_2 MQDs, the percentages of different particle size ranges were determined by using the software nano measurement. From Fig. 2B, the size distribution histogram of N-Ti_3C_2 MQDs displayed an average diameter of 5.0–5.8 nm. Meanwhile, the surface functional groups of N-Ti_3C_2 MQDs were analyzed with FT-IR (Fig. S4A) and XPS was used to investigate the valence states and elemental makeup of N-Ti_3C_2 MQDs (Fig. S4B). These findings demonstrated that the solvothermal treatment had produced oxygenous groups on the N-Ti_3C_2 MQDs surface, which is advantageous for their improved dispersion in aqueous solution [32, 33].

By capturing fluorescence emission spectra and UV–vis absorption spectra, the optical properties of N-Ti_3C_2 MQDs were examined. Figure 2C showed the strong absorption peak of ultraviolet light and the weak absorption peak of visible light of N-Ti_3C_2 MQDs (black line). In addition, N-Ti_3C_2 MQDs exhibited excitation-dependent fluorescence behavior similar to the previously reported Ti_3C_2 MQDs [34]. In accordance with Fig. 2C, the emission peak gradually red-shifted as different excitation wavelengths changed continuously. The brightest fluorescence peak of N-Ti_3C_2 MQDs was found at about 430 nm when the excitation wavelength was 340 nm. The maximum excitation wavelength was set at 380 nm to balance the fluorescence intensity in this study. At the same time, N-Ti_3C_2 MQDs synthesized exhibited excellent optical stability. As shown in Fig. S5 and Fig. 2D, the fluorescence intensity of N-Ti_3C_2 MQDs did not change significantly at different pH, different temperatures, and continuous scanning for 1 h (excitation at 380 nm).

Feasibility and mechanism of FA detection by MON system

MIL-53(Fe)-NO_2 with oxidation-like activity can catalyze OPD to produce DAP, a yellow oxidized product with an emission at 560 nm. N-Ti_3C_2 MQDs display blue fluorescence at 450 nm. DAP can quench the blue fluorescence of N-Ti_3C_2 MQDs through IFE since its absorption spectrum overlaps with the emission spectrum of N-Ti_3C_2 MQDs obviously. However, FA can interact with OPD to generate Schiff base, which reduces the amount of free OPD in

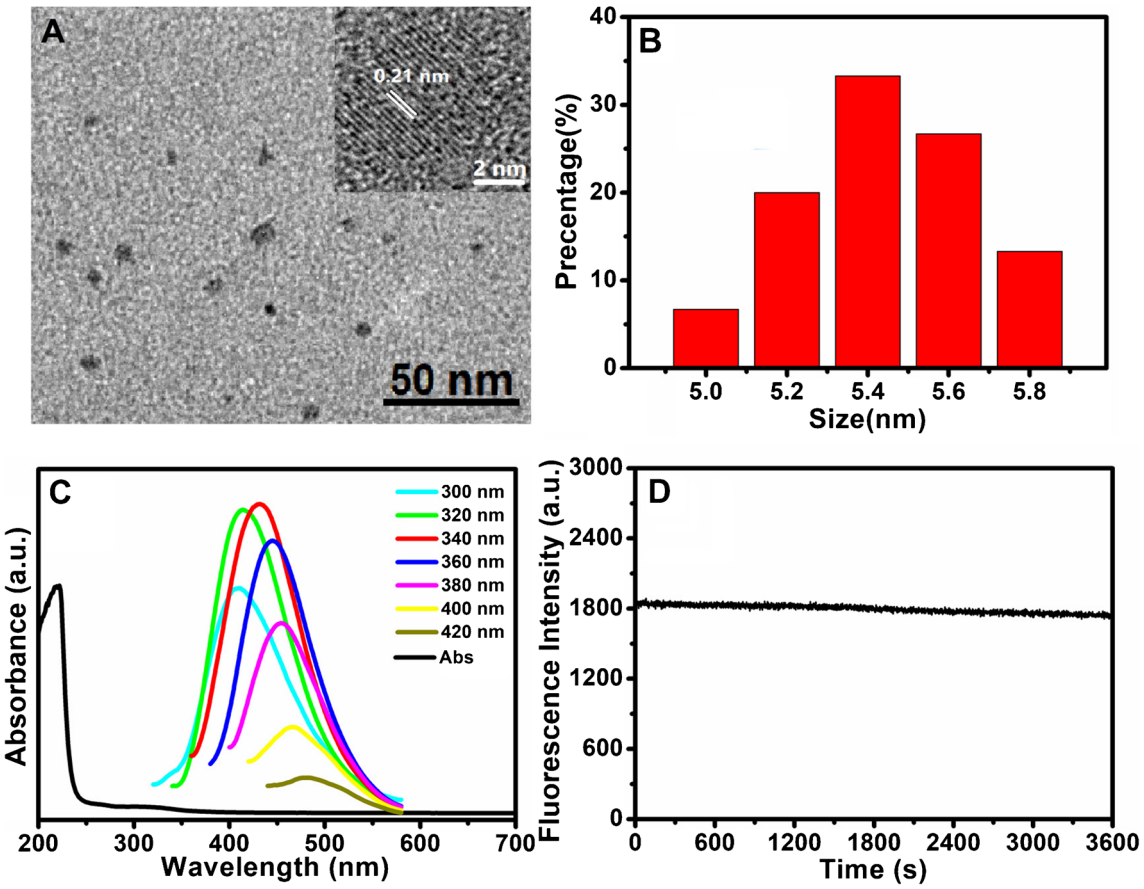

Fig. 2 **A** TEM image; inset: high-resolution TEM image and **B** size distribution histogram of N-Ti_3C_2 MQDs. **C** Fluorescent emission spectra of N-Ti_3C_2 MQDs at various excitation wavelengths and their UV–vis absorption spectra. The images taken in visible light (left) and UV light (right) are shown in the inset. **D** Fluorescence stability of N-Ti_3C_2 MQDs excited at 380 nm for 3600 s

the system that can be catalyzed by MIL-53(Fe)-NO_2, so that the luminescence at 560 nm is weakened, and the luminescence in the 450 nm band is restored. In terms of the description above, a ratio fluorescence sensor for FA detection was constructed (Scheme 1). Based on the proportion of the fluorescence intensities of N-Ti_3C_2 MQDs and DAP, an understandable signal for FA detection was created.

Through a series of experiments, the working mechanism of the sensor was verified. Figure 3A exhibited that the luminescence intensity of N-Ti_3C_2 MQDs alone reached the maximum at 450 nm. When N-Ti_3C_2 MQDs were separately mixed with MIL-53(Fe)-NO_2, OPD, and FA, their luminescence intensity remained basically unchanged. The fluorescence spectra of MIL-53(Fe)-NO_2 and OPD showed that DAP had a significant fluorescence emission peak at 560 nm. However, the fluorescence intensity of N-Ti_3C_2 MQDs reduced at 450 nm and a new fluorescence peak emerged at 560 nm when MIL-53(Fe)-NO_2 and OPD were added simultaneously. The fluorescence at 450 and 560 nm was recovered and weakened, respectively, when FA was present in the system.

We intended to conduct an in-depth discussion on the quenching mechanism of N-Ti_3C_2 MQDs induced by DAP. We firstly verified that N-Ti_3C_2 MQDs did not have the ability to catalyze OPD oxidation (Fig. S6). However, the DAP generated in the system was obtained from the oxidation of OPD catalyzed by MIL-53(Fe)-NO_2. Figure 3B illustrated that there was a substantial overlap between the DAP absorption spectra and the N-Ti_3C_2 MQDs emission spectrum. Additionally, the combination of N-Ti_3C_2 MQDs and DAP did not appreciably alter the absorption spectra of DAP, demonstrating that the two substances did not react to produce new molecules. Furthermore, the fluorescence lifetime of N-Ti_3C_2 MQDs stayed pretty much the same after DAP addition, indicating the existence of static quenching process (Fig. 3C). By the way, the zeta potentials of MIL-53(Fe)-NO_2, DAP, and N-Ti_3C_2 MQDs were 14.7, – 6.22, and – 14.9 mV, respectively (Fig. 3D), excluding the possibility of electrostatic attraction between DAP and N-Ti_3C_2 MQDs. These findings demonstrated that IFE induced DAP quenching of N-Ti_3C_2 MQDs

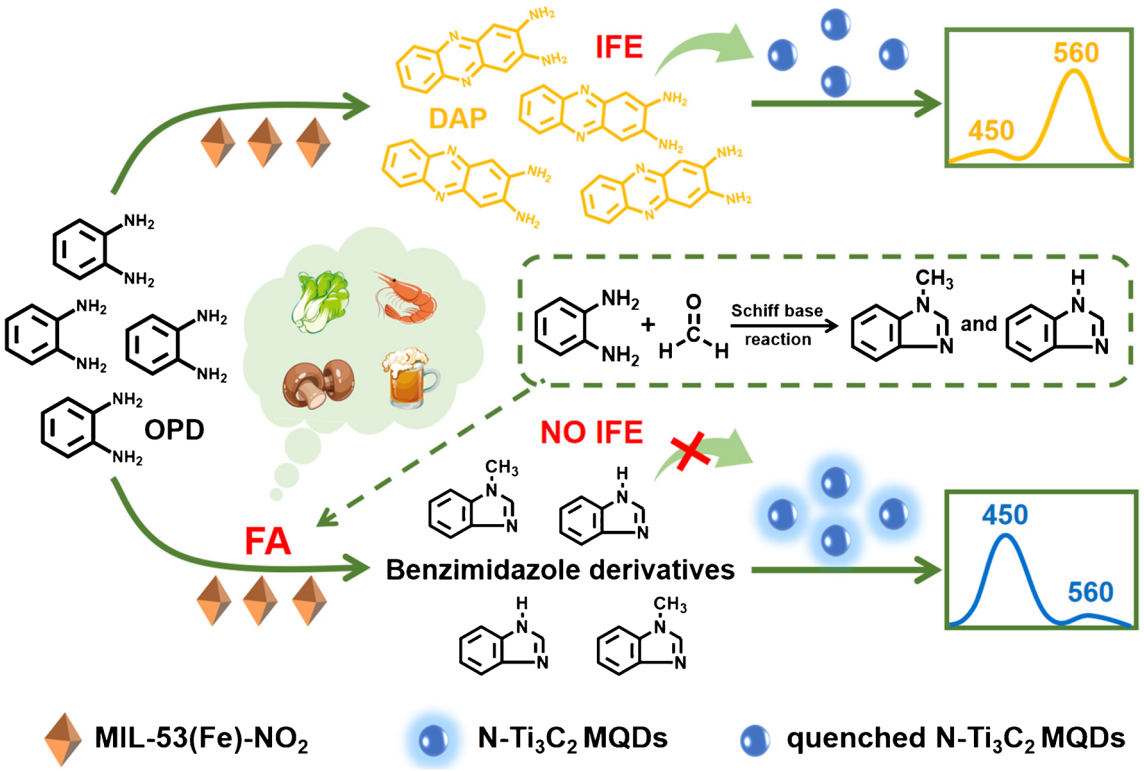

Scheme 1 Schematic diagram of FA detection by ratio fluorescence method based on MON system. Dashed box: specific Schiff base reaction of FA with OPD

fluorescence. According to the aforementioned results, FA might be identified by our ratio fluorescence sensor.

Optimization of experimental conditions

So as to achieve optimum conditions for FA detection by MON system, the effects of pH, temperature, OPD concentration, MIL-53(Fe)-NO_2 concentration, incubation time, and reaction time on the MON system were investigated. $F_{with}/F_{without}$ (F_{with} and $F_{without}$ represented the ratio of F_{450} to F_{560} in the respective presence and absence of target FA) was used as an evaluation criterion. pH was a crucial detection factor. It can be seen from Fig. S7A that $F_{with}/F_{without}$ reached its peak at pH 4.5. The reason is that nanozymes prefer to perform activity in acidic solutions through pre-absorption of H^+ and base-like decomposition of H_2O_2 and O_2 [35]. The temperature had a great effect upon the reaction rate and stability. It was manifested from Fig. S7B that when the temperature went up, MIL-53(Fe)-NO_2's catalytic activity increased significantly and peaked at 37 ℃. On the contrary, with the further increase of temperature, $F_{with}/F_{without}$ gradually decreased. It may be that too high temperature destroyed the structure and activity of MIL-53(Fe)-NO_2, thus inhibiting the production of DAP. In addition, the concentration of OPD was also important in detection. When the concentration of OPD increased to 0.04 mM, the value of $F_{with}/F_{without}$ reached its maximum, indicating that this concentration was sufficient to react with the target substance, and further increase would not cause significant changes in the value of $F_{with}/F_{without}$ (Fig. S7C). Figure S7D showed that $F_{with}/F_{without}$ gradually increased when MIL-53(Fe)-NO_2 concentration increased. When MIL-53(Fe)-NO_2 concentration reached 40 μg·mL^{-1}, there was no significant change in $F_{with}/F_{without}$ value, indicating that 40 μg·mL^{-1} MIL-53(Fe)-NO_2 was sufficient to detect FA. Time also had a certain influence on the intensity of fluorescence. Figures S7E and S7F clearly showed that 30 min was the best time for the incubation of OPD with FA, and the 40 min was the most suitable time for MIL-53(Fe)-NO_2 to catalyze the production of DAP from OPD. Further extension of the reaction time did not lead to significant changes in $F_{with}/F_{without}$. The catalytic activity of MIL-53(Fe)-NO_2 was significantly influenced by its concentration. Combined with the above results, the optimal pH, temperature, OPD concentration, MIL-53(Fe)-NO_2 concentration, incubation time, and reaction time were pH 4.5, 37 ℃, 0.04 mM, 40 μg·mL^{-1}, 30 min, and 40 min, respectively.

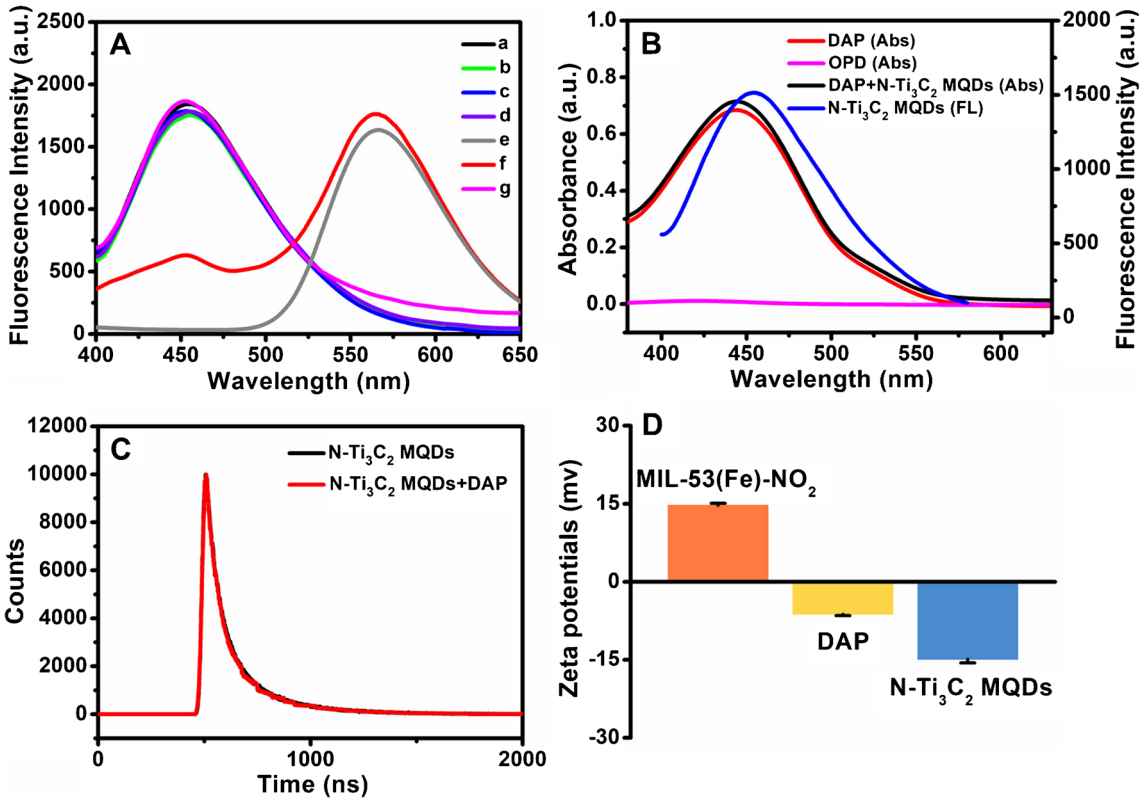

Fig. 3 **A** Fluorescence spectra (a) $N\text{-}Ti_3C_2$ MQDs, (b) FA + $N\text{-}Ti_3C_2$ MQDs, (c) OPD + $N\text{-}Ti_3C_2$ MQDs, (d) MIL-53(Fe)-NO_2 + $N\text{-}Ti_3C_2$ MQDs, (e) MIL-53(Fe)-NO_2 + OPD, (f) MIL-53(Fe)-NO_2 + OPD + $N\text{-}Ti_3C_2$ MQDs, (g) MIL-53(Fe)-NO_2 + OPD + FA + $N\text{-}Ti_3C_2$ MQDs. **B** UV–vis absorption (Abs) spectra of OPD, DAP, and DAP + $N\text{-}Ti_3C_2$ MQDs, and the fluorescence spectrum (FL) of $N\text{-}Ti_3C_2$ MQDs. **C** The fluorescence lifetime spectra of $N\text{-}Ti_3C_2$ MQDs and $N\text{-}Ti_3C_2$ MQDs + DAP. **D** The zeta potential histogram of MIL-53(Fe)-NO_2, DAP, and $N\text{-}Ti_3C_2$ MQDs ($n = 3$)

Methodological validation of MON system

FA was detected under the ideal experimental circumstances. Figure 4A demonstrated that the quenching fluorescence of $N\text{-}Ti_3C_2$ MQDs was restored when the concentration of FA steadily increased while the fluorescence of DAP decreased. F_{450}/F_{560} as the fluorescence intensity ratio was linearly correlated with the concentration of FA within 1–200 μM, but

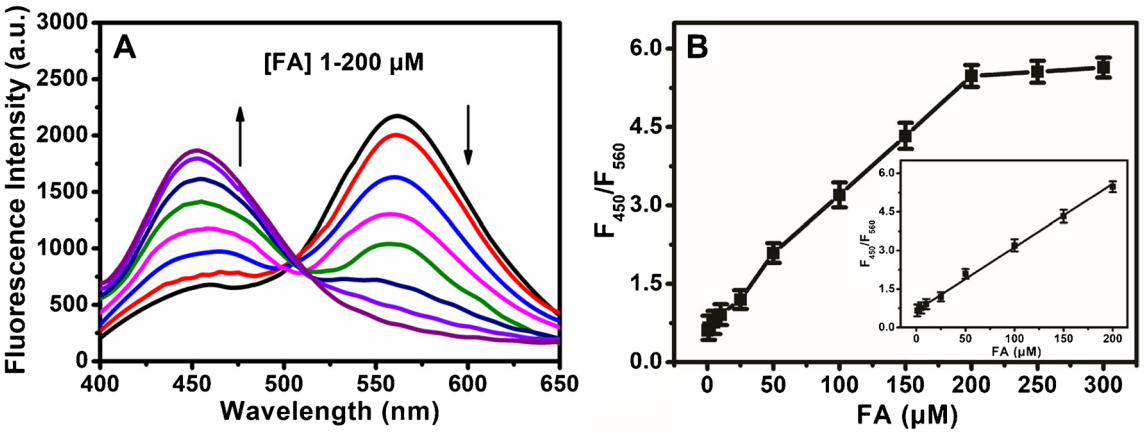

Fig. 4 **A** The MON system's fluorescence spectra at various FA concentrations. **B** The relationship between the F_{450}/F_{560} ratio and FA concentration. Inset: the standard curve of FA detection (1–200 μM) ($n = 3$)

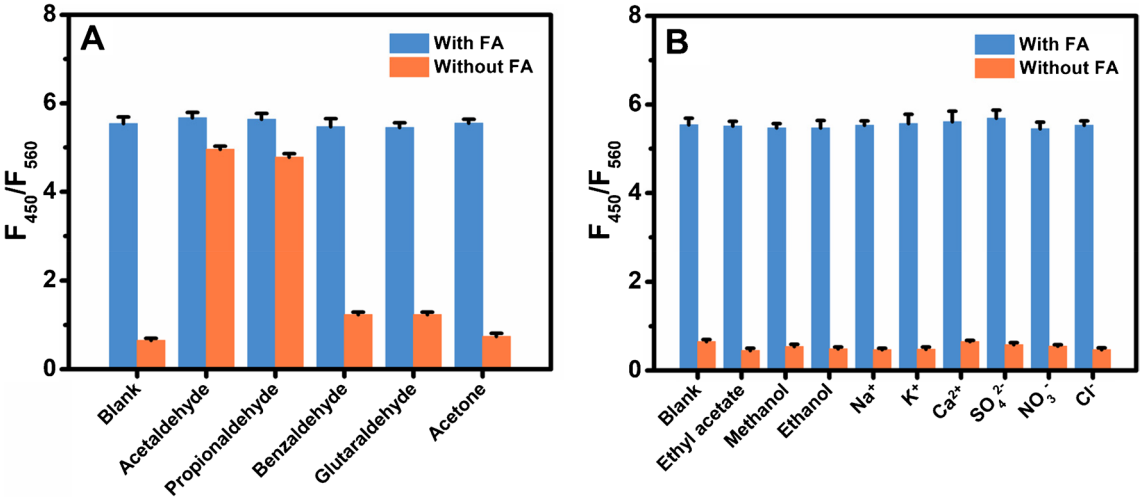

Fig. 5 **A** Selectivity of FA detection toward aldehydes and ketones. **B** Anti-interference toward small molecules and inorganic ions. The concentration of FA was 200 μM, and the concentrations of aldehydes were 600 μM. The concentrations of other potential interferences were all 2 mM ($n = 3$)

the fluorescence intensity ratio did not alter much when the concentration of FA increased further (Fig. 4B). This may be due to the constant concentration of OPD in the system, and when all OPD react with FA, the further addition of FA has little effect on the fluorescence of the system. The limit of detection for FA is 0.49 μM according to the 3σ rule. Compared with FA detection methods reported in the literature (Table S2), the MON system had a relatively wide linear range and a relatively low detection limit, which was attributed to the specific Schiff base reaction of FA with OPD and the construction of a rate-type fluorescent probe. Table S3 showed that within-run and between-run relative standard deviations (RSD) obtained at low, medium, and high FA concentration levels were less than 4.7% and 5.4%, respectively. These outcomes indicated that MON system designed had good repeatability and reproducibility when it came to FA.

To evaluate the MON system's specificity for FA, substances that may interfere with FA detection were selected, including aldehydes, ketones, organic molecules, and common ions. As shown in Fig. 5, most potential interfering substances had negligible effects. Although other aldehydes interfered with the detection of FA to a certain extent, the concentration of FA was much higher than that of other aldehydes in atmosphere, food, and other environmental media, so this method has good selectivity for FA detection in food.

FA detection in food samples

Frozen shrimp, cabbage, mushroom, and beer were selected to further evaluate the feasibility of MON system for FA detection by standard addition. According to Table S4, the recoveries of FA samples at various concentrations ranged from 98.7 to 102% with RSD less than 3.9%, revealing the feasibility of the method built. Low concentrations of FA were detected in frozen shrimp, cabbage, and mushroom all after treatment, which may be related to endogenous formaldehyde. Researchers have found that trimethylamine oxide in fish, shrimp, shellfish, and other aquatic products can be decomposed into dimethylamine and FA under the action of enzymes [36]. In addition, FA is a by-product of the breakdown of lentinan acid into lentinan flavor product which is lentinan essence [37]. FA concentration in beer sample was 1.08 μM, which was lower than the national standard limit of FA concentration of 2 $mg \cdot L^{-1}$ (66.7 μM) [6].

Table 1 Comparison of the results of MON and HPLC for FA detection ($n = 3$)

Samples	MON system (μM)	HPLC values (μM)	Relative error (%)
Frozen shrimp	5.71	5.64	1.2
	8.67	8.58	1.0
	108	107	0.9
	167	166	0.6
Cabbage	0.752	0.767	−2.0
	3.81	3.88	−1.8
	100	99.0	1.0
	161	162	−0.6
Mushroom	18.2	17.8	2.2
	21.3	20.7	1.9
	119	116	2.6
	179	178	1.1
Beer	1.08	1.13	−4.6
	4.14	4.19	−1.2
	101	103	−2.0
	160	161	−0.6

The same batches of food samples were also tested by HPLC to verify the accuracy of MON system (Table S5), and there was no significant difference between two means taken together. The aforementioned results demonstrated that the MON system had good sensitivity and accuracy in detecting FA in food samples (Table 1).

Conclusions

On the whole, we used the method of combining MIL-53(Fe)-NO_2 and N-Ti_3C_2 MQDs to form the ratio fluorescent probe by interacting the fluorescence of DAP and N-Ti_3C_2 MQDs. Based on the stability of N-Ti_3C_2 MQDs fluorescence, the amplification effect of ratio fluorescence on the target signal, and the specific reaction between FA and OPD, the highly sensitive determination of FA was achieved. Compared with the traditional single-signal detection method, it has the advantages of high sensitivity, good selectivity, simple detection, and can reduce the interference from probe concentration, light source, instrument efficiency, and measurement conditions. It can be directly applied to the detection of FA in food. The whole testing process is environmentally friendly, safe, and convenient. However, there are some limitations to this work. Although MIL-53(Fe)-NO_2 showed higher oxidase-like activity and reduced the use of hydrogen peroxide, the detection time was still long, which was not conducive to real-time detection. In addition, the MON system cannot yet be converted into a portable device in visual or digital format, which limits the field inspection of the method. Therefore, the improvement of nanozyme activity and the opening of visualization equipment will be the direction of our further exploration.

Supplementary Information The online version contains supplementary material available at https://doi.org/10.1007/s00604-024-06348-7.

Funding This work was supported by the National Natural Science Foundation of China (No. 81973283, 61775099, 21705080); Natural Science Foundation of Jiangsu Province (No. BK20221304, BK20171487, BK20171043); "Blue Project" Foundation of the Higher Education Institutions of Jiangsu Province; Key project of connotation construction of Nanjing Medical University; and Shandong Key Laboratory of Biochemical Analysis (SKLBA2303).

Data Availability Many thanks to the editors for their attention and recognition of our research work. We fully understand the journal's request for data sharing, but due to our lab's policies and confidentiality agreements, we cannot provide raw data. So the data availability statement does not apply to this article. However, we have fully described the details of the experiment in the paper, and if editors or reviewers have questions about specific data, we will try to provide more detailed explanations and explanations.

Declarations

Ethical approval This research did not involve human or animal samples.

Conflict of interest The authors declare no competing interests.

References

1. Wang X, Rehman A, Kong R, Cheng Y, Tian X, Liang M, Zhang L, Xia L, Qu F (2021) Naphthalimide derivative-functionalized metal-organic framework for highly sensitive and selective determination of aldehyde by space confinement-induced sensitivity enhancement effect. Anal Chem 93:8219–8227. https://doi.org/10.1021/acs.analchem.1c00916
2. Zhao X, Ji C, Ma L, Wu Z, Cheng W, Yin M (2018) An aggregation-induced emission-based 'turn-on' fluorescent probe for facile detection of gaseous formaldehyde. ACS Sens 3:2112–2117. https://doi.org/10.1021/acssensors.8b00664
3. Wahed P, Razzaq MA, Dharmapuri S, Corrales M (2016) Determination of formaldehyde in food and feed by an in-house validated HPLC method. Food Chem 202:476–483. https://doi.org/10.1016/j.foodchem.2016.01.136
4. Zhao Q, Shen T, Liu Y, Hu X, Zhao W, Ma Z, Li P, Zhu X, Zhang Y, Liu M, Yao S (2021) Universal nanoplatform for FA detection based on the oxidase-mimicking activity of MnO_2 nanosheets and the in situ catalysis-produced fluorescence species. J Agric Food Chem 69:7303–7312. https://doi.org/10.1021/acs.jafc.1c01174
5. Borah N, Gogoi D, Ghosh NN, Tamuly C (2023) GA-AuNP@Tollens' complex as a highly sensitive plasmonic nanosensor for detection of formaldehyde and benzaldehyde in preserved food products. Food Chem 399:133975. https://doi.org/10.1016/j.foodchem.2022.133975
6. Luong J, Yang X, Hua Y, Yang P, Gras R (2018) Gas chromatography with in situ catalytic hydrogenolysis and flame ionization detection for the direct measurement of formaldehyde and acetaldehyde in challenging matrices. Anal Chem 90:13855–13859. https://doi.org/10.1021/acs.analchem.8b04563
7. Yuan C, Pu J, Fu D, Min Y, Wang L, Liu J (2022) UV-vis spectroscopic detection of formaldehyde and its analogs: a convenient and sensitive methodology. J Hazard Mater 438:129457. https://doi.org/10.1016/j.jhazmat.2022.129457
8. Dugheri S, Massi D, Mucci N, Marrubini G, Cappelli G, Speltini A, Bonferoni MC, Arcangeli G (2021) Exposure to airborne formaldehyde: sampling and analytical methods-a review. Trends Environ Anal Chem 29:e00116. https://doi.org/10.1016/j.teac.2021.e00116
9. Nie X, Chen Z, Tian Y, Chen S, Qu L, Fan M (2021) Rapid detection of trace formaldehyde in food based on surface-enhanced Raman scattering coupled with assembled purge trap. Food Chem 340:127930. https://doi.org/10.1016/j.foodchem.2020.127930
10. Zhang J, Lv F, Li Z, Jiang G, Tan M, Yuan M, Zhang Q, Cao Y, Zheng H, Zhang L, Tang C, Fu W, Liu C, Liu K, Gu L, Jiang J, Zhang G, Guo S (2022) Cr-doped Pd metallene endows a practical formaldehyde sensor new limit and high selectivity. Adv Mater 34:2105276. https://doi.org/10.1002/adma.202105276
11. Li J, Ding D, Wang J, Xu L, Tan D, Lin W (2022) Development of a multi-task formaldehyde specific fluorescent probe for bioimaging in living systems and decoration materials analysis. Chem Eng J 448:137634. https://doi.org/10.1016/j.cej.2022.137634
12. Yuan G, Ding H, Peng L, Zhou L, Lin Q (2020) A novel fluorescent probe for ratiometric detection of formaldehyde in real food samples, living tissues and zebrafish. Food Chem 331:127221. https://doi.org/10.1016/j.foodchem.2020.127221
13. Amer WA, Rehab AF, Abdelghafar ME, Torad NL, Atlam AS, Ayad MM (2021) Green synthesis of carbon quantum dots from purslane leaves for the detection of formaldehyde using quartz

crystal microbalance. Carbon 179:159–171. https://doi.org/10.1016/j.carbon.2021.03.047
14. Gao Y, Yu Z, Huang L, Zeng Y, Liu X, Tang D (2023) Photoinduced electron transfer modulated photoelectric signal: toward an organic small molecule-based photoelectrochemical platform for formaldehyde detection. Anal Chem 95:9130–9137. https://doi.org/10.1021/acs.analchem.3c01690
15. Akshath US, Bhatt P (2018) Supramolecular nano-sniffers for ultrasensitive detection of formaldehyde. Biosens Bioelectron 100:201–207. https://doi.org/10.1016/j.bios.2017.09.010
16. Che H, Li Y, Tian X, Yang C, Lu L, Nie Y (2021) A versatile logic detector and fluorescent film based on Eu-based MOF for swift detection of formaldehyde in solutions and gas phase. J Hazard Mater 410:124624. https://doi.org/10.1016/j.jhazmat.2020.124624
17. Chi J, Song Y, Feng L (2023) A ratiometric fluorescent paper sensor based on dye-embedded MOF for high-sensitive detection of arginine. Biosens Bioelectron 241:115666. https://doi.org/10.1016/j.bios.2023.115666
18. Ge J, Yang L, Li Z, Wan Y, Mao D, Deng R, Zhou Q, Yang Y, Tan W (2022) A colorimetric smartphone-based platform for pesticides detection using Fe-N/C single-atom nanozyme as oxidase mimetics. J Hazard Mater 436:129199. https://doi.org/10.1016/j.jhazmat.2022.129199
19. Gai P, Pu L, Wang C, Zhu D, Li F (2023) CeO2@NC nanozyme with robust dephosphorylation ability of phosphotriester: a simple colorimetric assay for rapid and selective detection of paraoxon. Biosens Bioelectron 220:114841. https://doi.org/10.1016/j.bios.2022.114841
20. Chang J, Yu L, Hou T, Hu R, Li F (2023) Direct and specific detection of glyphosate using a phosphatase-like nanozyme-mediated chemiluminescence strategy. Anal Chem 95:4479–4485. https://doi.org/10.1021/acs.analchem.2c05198
21. Yu K, Li M, Chai H, Liu Q, Hai X, Tian M, Qu L, Xu T, Zhang G, Zhang X (2023) MOF-818 nanozyme-based colorimetric and electrochemical dual-mode smartphone sensing platform for in situ detection of H_2O_2 and H_2S released from living cells. Chem Eng J 451:138321. https://doi.org/10.1016/j.cej.2022.138321
22. Wu J, Wang Z, Jin X, Zhang S, Li T, Zhang Y, Xing H, Yu Y, Zhang H, Gao X, Wei H (2021) Hammett relationship in oxidase-mimicking metal-organic frameworks revealed through a protein-engineering-inspired strategy. Adv Mater 33:2005024. https://doi.org/10.1002/adma.202005024
23. Bilal M, Singh AK, Iqbal HMN, Boczkaj G (2023) Enzyme-conjugated MXene nanocomposites for biocatalysis and biosensing. Chem Eng J 474:145020. https://doi.org/10.1016/j.cej.2023.145020
24. Yu L, Chang J, Zhuang X, Li H, Hou T (2022) Li F (2022) Two-dimensional cobalt-doped Ti3C2 MXene nanozyme-mediated homogeneous electrochemical strategy for pesticides assay based on in situ generation of electroactive substances. Anal Chem 94:3669–3676. https://doi.org/10.1021/acs.analchem.1c05300
25. Jiang D, Wei M, Du X, Qin M, Shan X, Chen Z (2022) One-pot synthesis of ZnO quantum dots/N-doped Ti_3C_2 MXene: tunable nitrogen-doping properties and efficient electrochemiluminescence sensing. Chem Eng J 430:132771. https://doi.org/10.1016/j.cej.2021.132771
26. Lu Q, Wang J, Li B, Weng C, Li X, Yang W, Yan X, Hong J, Zhu W, Zhou X (2020) Dual-emission reverse change ratio photoluminescence sensor based on a probe of nitrogen-doped Ti_3C_2 quantum dots@DAP to detect H_2O_2 and xanthine. Anal Chem 92:7770–7777. https://doi.org/10.1021/acs.analchem.0c00895
27. Zheng X, Qi S, Cao Y, Shen L, Au C, Jiang L (2021) Morphology evolution of acetic acid-modulated MIL-53(Fe) for efficient selective oxidation of H_2S. Chin J Catal 42:279–287. https://doi.org/10.1016/S1872-2067(20)63625-7
28. Chen Z, Su H, Sun P, Bai P, Yang J, Li M, Deng Y, Liu Y, Geng Y, Xu Y (2022) A nitroaromatic cathode with an ultrahigh energy density based on six-electron reaction per nitro group for lithium batteries. Proc Natl Acad Sci USA 119:e2116775119. https://doi.org/10.1073/pnas.2116775119
29. Li J, Gao M, Xia X, Cen Y, Wei F, Yang J, Wang L, Hu Q, Xu G (2023) Spherical hydrogel sensor based on PB@Fe-COF@Au nanoparticles with triplet peroxidase-like activity and multiple capture sites for effective detection of organophosphorus pesticides. ACS Appl Mater Interfaces 15:6473–6485. https://doi.org/10.1021/acsami.2c19921
30. Liu J, Ma W, Wang Y, Gu Q, Pan Q, Zong S, Qin M, Li J (2024) Enhanced oxidase-mimic constructed by luminescent carbon dots loaded on MIL-53(Fe)-NO_2 for dual-mode detection of gallic acid and biothiols in food and humans. Food Chem 433:137241. https://doi.org/10.1016/j.foodchem.2023.137241
31. Wang L, Zhang N, Li Y, Kong W, Gou J, Zhang Y, Wang LN, Yu G, Zhang P, Cheng H, Qu L (2021) Mechanism of nitrogen-doped Ti_3C_2 quantum dots for free-radical scavenging and the ultrasensitive H_2O_2 detection performance. ACS Appl Mater Interfaces 13:42442–42450. https://doi.org/10.1021/acsami.1c11242
32. Yang J, Chen L, Qi J, Luo F, Li L, Wu H, Cao F, Gu J (2024) Acid-assisted ultrasonic preparation of nitrogen-doped MXene quantum dots for the efficient fluorescence "off-on-off" detection of Zn(II) in water and oxalic acid in vegetables. Food Chem 430:137007. https://doi.org/10.1016/j.foodchem.2023.137007
33. Gou J, Zhao L, Li Y, Zhang J (2021) Nitrogen-doped Ti_2C MXene quantum dots as antioxidants. ACS Appl Nano Mater 4:12308–12315. https://doi.org/10.1021/acsanm.1c02783
34. Nie Y, Liang Z, Wang P, Ma Q, Su X (2021) MXene-derived quantum dot@gold nanobones heterostructure-based electrochemiluminescence sensor for triple-negative breast cancer diagnosis. Anal Chem 93:17086–17093. https://doi.org/10.1021/acs.analchem.1c04184
35. Chen L, Xing S, Lei Y, Chen Q, Zou Z, Quan K, Qing Z, Liu J, Yang R (2021) Glucose-powered activatable nanozyme breaking pH and H_2O_2 limitations for treating diabetic infections. Angew Chem Int Ed 60:23534–23539. https://doi.org/10.1002/anie.202107712
36. Sibirny V, Demkiv O, Klepach H, Honchar T, Gonchar M (2011) Alcohol oxidase- and formaldehyde dehydrogenase-based enzymatic methods for formaldehyde assay in fish food products. Food Chem 127:774–779. https://doi.org/10.1016/j.foodchem.2010.12.146
37. Liu Y, Yuan Y, Lei X, Yang H, Ibrahim SA, Huang W (2013) Purification and characterisation of two enzymes related to endogenous formaldehyde in Lentinula edodes. Food Chem 138:2174–2179. https://doi.org/10.1016/j.foodchem.2012.12.038